RSC Advances

PAPER

View Article Online
View Journal | View Issue

Cite this: *RSC Adv.*, 2019, **9**, 5834

Mussel-inspired nano-silver loaded layered double hydroxides embedded into a biodegradable polymer matrix for enhanced mechanical and gas barrier properties

Long Mao,[ab] Jing-yi Liu,[a] Si-jie Zheng,[a] Hui-qing Wu,*[c] Yue-jun Liu,*[ab] Zhi-han Li[b] and Yong-kang Bai[d]

In this paper, a facile, green and mussel-inspired method is presented to prepare silver loaded layered double hydroxides (Ag-LDHs@PDA and Ag-LDHs@TA–Fe(III)) using a pre-synthesis polydopamine (PDA)/tannic acid (TA)–Fe(III) layer as a nanoscale guide and PDA/TA itself as a reducing reagent to form uniform silver nanoparticles (AgNPs) on the surface of modified LDHs. Meanwhile, another kind of LDH, Ag-LDHs(PVP), was prepared *via* the direct reduction of the precursor $[Ag(NH_3)_2]^+$ with polyvinyl pyrrolidone (PVP). And three kinds of Ag-LDHs/poly(ε-caprolactone) (PCL) nanocomposite were prepared by blending Ag-LDHs and pure PCL *via* a solution casting method to obtain homogeneous films. It is shown that the obtained AgNPs are distributed on the LDH surfaces uniformly. And the high loading and medium size of the AgNPs present in Ag-LDHs(PVP) give it the best antibacterial properties. However, compared with Ag-LDHs(PVP), the better dispersibilities of Ag-LDHs@PDA and Ag-LDHs@TA–Fe(III) contribute to the greater aspect ratios of Ag-LDHs in the matrices, resulting in an increase in the number of tortuous paths for gas diffusion. Meanwhile, Ag-LDHs@PDA and Ag-LDHs@TA–Fe(III) have stronger interactions with the PCL matrix, which is favorable for the existence of less interface defects in the matrix, resulting in an improvement in the mechanical and gas barrier properties. Therefore, mussel-inspired antibacterial Ag-LDHs/PCL nanocomposites show preferable mechanical and gas barrier properties.

Received 22nd November 2018
Accepted 4th February 2019

DOI: 10.1039/c8ra09602c

rsc.li/rsc-advances

1. Introduction

Layered double hydroxides (LDHs), known as a kind of multifunctional anionic layered clay, can be expressed *via* the general formula $[M_{1-x}^{2+}M_x^{3+}(OH)_2]^{x+}(A_{x/n}^{n-})\cdot mH_2O$, where M^{2+} and M^{3+} occupy the octahedral holes in a brucite $[Mg(OH)_2]$-like layer, and A^{n-} exists between the hydrated interlayer galleries.[1] Among the layered clays, as a result of their synthetic origin, LDHs present many advantages, such as high specific surface areas, chemical purity, homogeneous structures and tunable chemical compositions.[2,3] LDHs have many multifunctional properties that make them attractive for practical applications, including use in nanomedicine, as catalyst supports, as functional additives, in water pollution treatment, and so on.[3]

In general, organic coatings are commonly applied to modify clay to improve the interfacial compatibility between clay minerals and matrices. Inspired by the versatile adhesion capabilities of marine adhesive proteins, polyphenolic compound surface modifications have been discovered as a powerful method to form adhesive and multifunctional coatings (such as polydopamine (PDA) and tannic acid (TA)–Fe(III) complexes) on almost any substrate, such as metal oxides, clay and fibers.[4,5] According to the literature,[6–10] PDA is capable of interacting strongly with polymers *via* hydrogen bonds and covalent bonds, hence, it can act as a bridge at organic–inorganic interfaces. Therefore, LDHs@PDA has been prepared *via* growing PDA *in situ* onto LDH surfaces.[6,7] And PDA coatings can further improve the dispersibility and interfacial interactions of LDHs in polymer matrices, correspondingly improving the properties. To the best of our knowledge, the surface modification of LDHs using a TA–Fe(III) complex has been seldom reported. According to previous studies,[11,12] TA can provide polydentate ligands for metal ions to form uniform TA–Fe(III) coatings rapidly due to the strong chelating ability of TA.[12–14]

[a]*Fujian Provincial Key Laboratory of Functional Materials and Applications, School of Materials Science and Engineering, Xiamen University of Technology, Ligong Road No. 600, Jimei District, Xiamen 361024, PR China. E-mail: yjliu_2005@126.com*

[b]*Key Laboratory of Advanced Packaging Materials and Technology of Hunan Province, Hunan University of Technology, Zhuzhou 412007, PR China*

[c]*College of Chemistry, Chemical Engineering and Biotechnology, Donghua University, Shanghai 201620, PR China. E-mail: Honeywhq@126.com*

[d]*Institute of Polymer Science in Chemical Engineering, Xi'an Jiao Tong University, Xi'an 710049, PR China*

These brilliant works have inspired us to consider the possibility of employing a TA–Fe(III) complex as an effective and functional coating on the surface of LDHs. Meanwhile, compared with PDA, TA–Fe(III) is relatively cheap and readily available, making its widespread application possible.[15] Therefore, we proposed a facile, green and mussel-inspired method to prepare surface modified LDHs coated by TA–Fe(III) (LDHs@TA–Fe(III)) *in situ* for the first time in our previous publication.[16]

In recent years, nanostructured materials have been considered as promising candidates to act as novel antibacterial agents in the functional materials field, owing to their unique physical and chemical properties. Many nanostructured materials (such as TiO_2, ZnO, gold and Ag) have been intensively investigated.[1,17,18] Among these, Ag-based nanomaterials have been extensively used as effective antibacterial agents against a wide range of microorganisms (*e.g.*, bacteria, fungi and viruses), because of the relatively low toxicity of silver to humans. Previous research has revealed that Ag nanoparticles (AgNPs) can directly react with proteins containing sulfur both inside and outside the cytomembranes of bacteria, causing structural changes or functional damage to the cytomembranes of bacteria and further affecting the viability of the bacterial cells.[17,19–22] According to previous studies,[23,24] polyphenolic compounds (*e.g.*, PDA and TA) can be used as active templates for the synthesis of AgNPs due to their abundant catechol and amine groups, and they exhibit extraordinary active features, such as excellent adhesive and reducing abilities. To summarize, polyphenolic coatings are able to act as reductants, binding reagents and universal platforms for secondary reactions. Hence, PDA/TA–Fe(III) coatings can provide an excellent platform to bind and reduce silver precursor $[Ag(NH_3)_2]^+$ ions *in situ* into metallic AgNPs on LDHs (named Ag-LDHs@PDA and Ag-LDHs@TA–Fe(III)), as shown in Scheme 1. To the best of our knowledge, compared with Ag-LDHs@PDA, Ag-LDHs@TA–Fe(III) prepared *via* this method has been rarely reported. Meanwhile, for comparison, Ag-LDHs(PVP) was prepared *via* the direct reduction of silver precursor $[Ag(NH_3)_2]^+$ ions with polyvinyl pyrrolidone (PVP). Ag-LDHs@PDA, Ag-LDHs@TA–Fe(III) and Ag-LDHs(PVP) are collectively known as Ag-LDHs in this paper.

Aliphatic polyesters are recognized as some of the most promising materials to act as the main sources of environmentally friendly biodegradable plastics.[25] Poly(ε-caprolactone) (PCL) is a linear and semicrystalline aliphatic polyester that can be slowly degraded by microorganisms.[26] The excellent physical properties, biological compatibility and commercial availability of PCL make it an attractive substitute for conventional non-biodegradable polymers, giving rise to common applications (*e.g.* packaging, biomedicine and agriculture). However, for practical applications of PCL, specific packaging requirements need to be satisfied (*e.g.* antibacterial and gas barrier properties).[27] In order to satisfy these requirements, three kinds of Ag-LDHs were applied to modify the PCL matrix. Therefore, antibacterial Ag-LDHs/PCL nanocomposites were prepared *via* a solution casting method to obtain homogeneous films. The purpose of our research is to provide more selectivity for the multifunctional modification of LDHs, to improve the interface compatibility of Ag loaded LDHs, and promote the application of LDHs for aliphatic polyester use.

2. Experimental section

2.1. Materials

MgAl-LDHs was prepared *via* a modified urea method followed by hydrothermal treatment.[6] Tannic acid (TA, analytical purity), $FeCl_3 \cdot 6H_2O$ (analytical purity), dopamine hydrochloride (DA, purity of over 98%), tris(hydroxymethyl)aminomethane (Tris, purity of over 99.9%), polyvinylpyrrolidone (PVP, average molecular weight = 24 000, K23-27), $AgNO_3$ (purity of over 98%), and $NH_3 \cdot H_2O$ (purity of over 25%) were purchased from Shanghai Aladdin Bio-Chem Technology Co., Ltd. Commercial poly(ε-caprolactone) (PCL, Capa™ 6800, $M_w \geq 80\,000$) was supplied by Perstorp. All other reagents were of analytical purity and used without further purification.

2.2. The preparation of Ag-LDHs

Original LDHs (MgAl-LDHs), LDHs@PDA and LDHs@TA–Fe(III) were synthesized using the methods reported in our previous publications.[6,16] Generally, LDHs@PDA (or LDHs@TA–Fe(III)) (0.1 g) was dispersed in ultrapure water (10 mL) under continuous sonication for 30 min. Freshly prepared $[Ag(NH_3)_2]^+$ ion solution (10 mL, 0.02 M) was dropwise added to the LDHs@PDA (or LDHs@TA–Fe(III)) dispersion under magnetic stirring, and the system was kept under stirring in an ice bath for 1 h. After centrifugation and washing with ultrapure water three times, the product was dried in a freeze dryer.

Ag-LDHs(PVP) was prepared *via* the direct reduction of the precursor $[Ag(NH_3)_2]^+$ with PVP. Generally, original LDHs (0.1 g) were dispersed in ultrapure water (10 mL) under continuous sonication for 30 min. Freshly prepared $[Ag(NH_3)_2]^+$ ion solution (10 mL, 0.02 M) was added to the LDH dispersion under magnetic stirring at room temperature for 1.5 h. Then, PVP aqueous solution (50 mL, 0.5 mM) was added for stabilization and reduction, and the product was stirred at 70 °C for 7 h. The product was collected *via* centrifugation and finally dried in a freeze dryer.

2.3. The preparation of Ag-LDHs/PCL nanocomposites

The mass fractions of Ag-LDHs in the Ag-LDHs/PCL nanocomposites were set to 0.5%, 1% and 3%, respectively. Ag-LDHs was dispersed in dimethyl formamide under continuous sonication for 30 min. Then commercial PCL was added to the dispersion at 40 °C under magnetic stirring for 1.5 h and the dispersion was heated to 80 °C under magnetic stirring for 1.5 h. Afterwards, the dispersion was treated with continuous sonication for 15 min. Finally, the dispersion was vaporized to obtain homogeneous films in horizontal PTFE molds at 60 °C.

2.4. Characterization

X-ray diffraction (XRD) patterns were recorded with a powder diffractometer (X'pert, Panalytical), using CuKα radiation at a scanning rate of 5° min^{-1} (from 10° to 80°). The microstructures of the Ag-LDHs/PCL nanocomposites were measured *via*

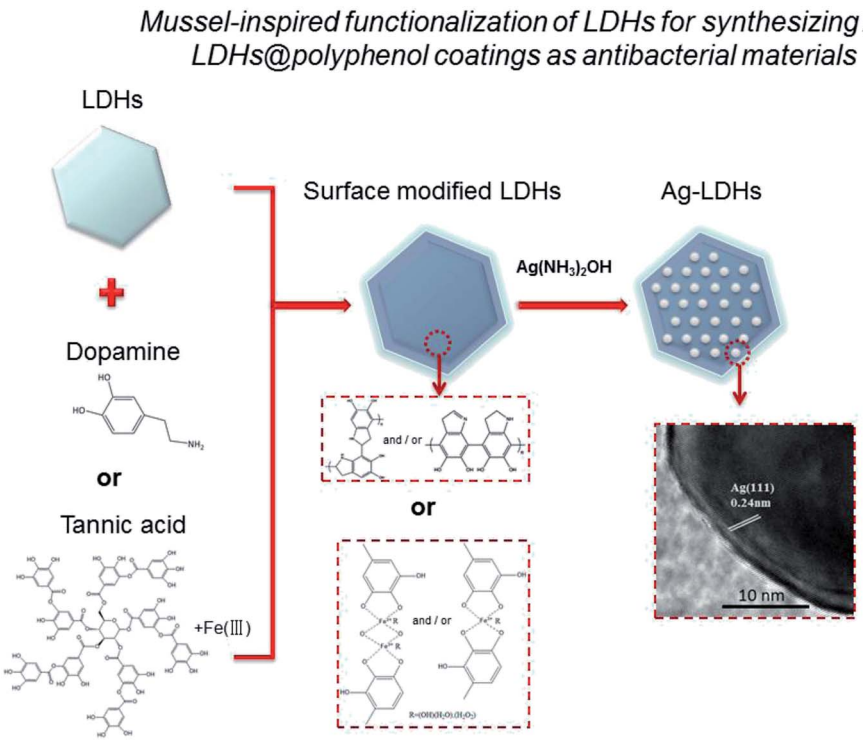

Scheme 1 A schematic illustration of the preparation of Ag-LDHs.

scanning electron microscopy (SEM, Sigma500, Zeiss). In order to maintain the original fractured surfaces of the Ag-LDHs/PCL nanocomposites, the samples were treated with liquid nitrogen to obtain fractured surfaces. The microstructure of Ag-LDHs was measured *via* transmission electron microscopy (TEM, Talos, FEI). And energy-dispersive X-ray spectrometry (EDS, X-Max^n, Oxford) measurements were taken using TEM and SEM to identify coatings around the original LDHs. UV-visible absorption spectra were recorded using a UV-visible spectrophotometer (SPECORD 210 PLUS, Analytik Jena) over the wavelength range of 300–800 nm. Thermal properties analysis was carried out with a differential scanning calorimeter (DSC, DSC214, Netzsch). The samples were heated from room temperature to 150 °C at 20 °C min^{-1} and kept at this temperature for 5 min to eliminate any thermal history. Then the samples were cooled down to −30 °C at a rate of 10 °C min^{-1} and heated to 150 °C at a rate of 10 °C min^{-1}. To estimate the crystallinity (χ) of the PCL matrix, the following equation was used: $\chi = [\Delta H_m/(\Delta H_0 \times \varphi)] \times 100\%$, where ΔH_m is the melting enthalpy, ΔH_0 is a reference value (136 J g^{-1})[28] that represents the melting enthalpy of a pure PCL crystal, and φ is the mass fraction of PCL in the composites. Thermal gravimetric analysis (TGA, TG209F3, Netzsch) was conducted from 30 to 800 °C under a N_2 atmosphere at a heating rate of 10 °C min^{-1}. The mechanical properties were measured on a micro-controlled electronic universal testing machine (ETM502B-Ex, Wance Technologies Ltd). Tensile test procedures followed the ISO 1184-1983 method. The gas barrier properties of samples were measured using an oxygen permeability tester (OX-TRAN 2/21, Mocon). Film specimens were cut into a circular shape with an area of 5 cm^3. The measurement environment was set at 23 ± 0.5 °C with 0.1 MPa oxygen pressure.

The minimum inhibitory concentration (MIC) method was carried out as follows. MIC values of Ag-LDHs were determined from the lowest concentration of Ag-LDHs that completely inhibited the growth of bacteria, *i.e.*, there was no visible formation of colonies as judged by the naked eye. The Gram negative bacteria strain *Escherichia coli* (*E. coli*) was first cultured for 12 h in a fluid nutrient medium. And then an appropriate bacterial suspension was diluted until the absorbance value was about 0.1 at a wavelength of 600 nm. After mixing 100 μL of bacteria suspension and 900 μL of fluid nutrient medium, Ag-LDHs powder with different concentrations ranging from 10 to 1000 μg mL^{-1} was dispersed uniformly in the bacteria suspensions and fluid nutrient medium. Then, the bacteria mixing liquid was placed in a constant temperature bath (37 °C) shaking bed for 2 h. Afterwards, the bacteria mixing liquid (0.1 mL) was coated evenly on the solid nutrient medium and incubated for 18 h at 37 °C. Finally, the MIC values of Ag-LDHs were determined using the solid nutrient medium without bacterial growth.

The antibacterial properties of the Ag-LDHs/PCL nanocomposites were evaluated against *E. coli* using the inhibition zones method. Before testing, the *E. coli* strain was first cultured in a flask, and then the prepared *E. coli* solution was pipetted onto a plate and spread over the surface. A circular disk of each membrane (d = 10 mm) was placed on the bacterial surface and incubated for 16 h at 37 °C. After that, the inhibition zones that formed around the films could serve as an indicator of the

antibacterial properties and these were visually observed with a digital camera.

3. Results and discussion

3.1. Structure of Ag-LDHs

Three kinds of Ag-LDHs were prepared *via* the reduction of a silver precursor, $[Ag(NH_3)_2]^+$ ions, with PVP, PDA and TA–Fe(III), respectively. TEM studies were carried out to investigate the morphology of AgNPs on the surface of the LDHs directly. After the reduction process, AgNPs are uniformly adsorbed on the surface of original LDHs, LDHs@PDA and LDHs@TA–Fe(III), leading to the formation of Ag-LDHs, as shown in Fig. 1. The average diameters of AgNPs on the LDHs can also be estimated as ~25, 65 and 15 nm, respectively, and, as shown in Fig. 2(a–c), AgNPs loading amounts on the LDHs are 3.37, 1.53 and 0.66 wt%, respectively. All Ag-LDHs samples possess Ag(111) crystal planes with a lattice spacing of 0.236 nm, as shown in the Fig. 2(d–f).[1] The successful preparation of AgNPs is further confirmed *via* XRD and UV-vis studies, as shown in Fig. 3. In Fig. 3(a), it can be seen that the diffraction reflections of LDHs are sharp and symmetrical, and the baselines are low and stable, indicating relatively well-formed crystalline layered structures. The (003), (006) and (110) characteristic diffraction peaks are easily recognized in all the patterns. XRD patterns of original LDHs and Ag-LDHs show almost identical characteristics to $MgAl–CO_3$ LDHs (JCPDS file no. 38-0487).[29] In addition to the characteristic diffraction peaks of the original LDHs, (111), (200), and (220) diffraction peaks of Ag are observed in the XRD patterns of Ag-LDHs.[30] This is consistent with the results from HRTEM images. As shown in Fig. 3(b), the original LDHs display no visible absorption peak between 300 and 800 nm. After loading AgNPs on the surface of the LDHs, there are strong absorption bands at ~420 and 444 nm.[31] This is characteristic of spherical AgNPs, due to surface plasmon resonance (SPR),[24] which further implies the formation of Ag-LDHs. The shapes, sizes and concentrations of nanoparticles, their morphologies and the reaction environments significantly affect the location and intensity of the SPR band. Compared with Ag-LDHs(PVP), Ag-LDHs@TA–Fe(III) shows a blue shift (from 444 nm to 420 nm), which strongly reveals an abrupt decrease in the dimensional size of AgNPs. Although AgNPs of LDHs@PDA have a larger size than those of Ag-LDHs(PVP), the concentration of AgNPs in Ag-LDHs@PDA is lower than that of AgNPs in Ag-LDHs(PVP). Compared with Ag-LDHs(PVP), Ag-LDHs@PDA still shows the blue shifting of the SPR band. In other words, a lower concentration of AgNPs may also lead to a blue shift in the SPR band.[17]

The photographs in Fig. 4 demonstrate the dispersibilities of LDHs and Ag-LDHs in aqueous solution. Original LDHs and three kinds of Ag-LDHs are respectively dispersed in ultrapure water *via* ultrasonication, and then the obtained dispersions are left to stand. After standing for 40 min, LDHs and Ag-LDHs(PVP) obviously aggregate and precipitate, while Ag-LDHs@PDA and Ag-LDHs@TA–Fe(III) stay homogenously dispersed. After standing for 120 min, LDHs and Ag-LDHs(PVP) completely precipitate, while Ag-LDHs@PDA and Ag-LDHs@TA–Fe(III) stay uniformly dispersed. The rather good dispersibilities of Ag-LDHs@PDA and Ag-LDHs@TA–Fe(III) can be attributed to the decreased surface energies of PDA and TA–Fe(III), which are wrapped on the surface of the original LDHs;[16] this can further improve the dispersibilities of Ag-LDHs@PDA and Ag-LDHs@TA–Fe(III) in the polymer matrix and correspondingly their performances.

3.2. Antibacterial properties of Ag-LDHs and Ag-LDHs/PCL nanocomposites

The minimum inhibitory concentrations (MICs) that would completely inhibit any visible growth of bacteria after overnight incubation have been quantified for Ag-LDHs. The differences in MIC values obtained are shown in Fig. 5. There is a general consensus that agrees that Ag ions released from unstable AgNPs are responsible for its excellent antibacterial activity. High antibacterial activity performance is obtained if the AgNPs have a large surface area. A larger surface area contributes to the release of more Ag ions; as a result, more are exposed to bacteria. Therefore, the order of antimicrobial activity was correlated to the quantity of silver loading and the size of AgNPs. The test results can be directly correlated with the loading of AgNPs confirmed *via* EDS results and the sizes of AgNPs confirmed by TEM. The dependence of the antibacterial activity on these parameters has been previously reported.[17] The medium size of the AgNPs present in Ag-LDHs(PVP) and the fact that it has the highest loading lead to it showing the best antibacterial properties. And the small size of the AgNPs present in Ag-LDHs@TA–Fe(III) and the fact that it has the lowest loading lead to it having the second-best antibacterial properties. Naturally, the large size of the AgNPs and the medium loading present in Ag-LDHs@PDA lead to it having the worst

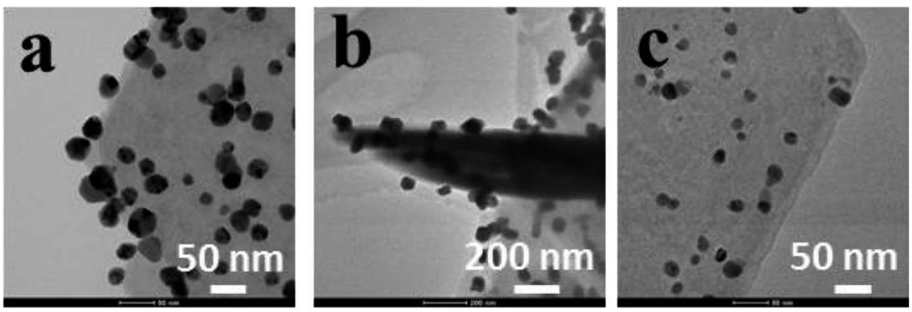

Fig. 1 TEM images of (a) Ag-LDHs(PVP), (b) Ag-LDHs@PDA and (c) Ag-LDHs@TA–Fe(III).

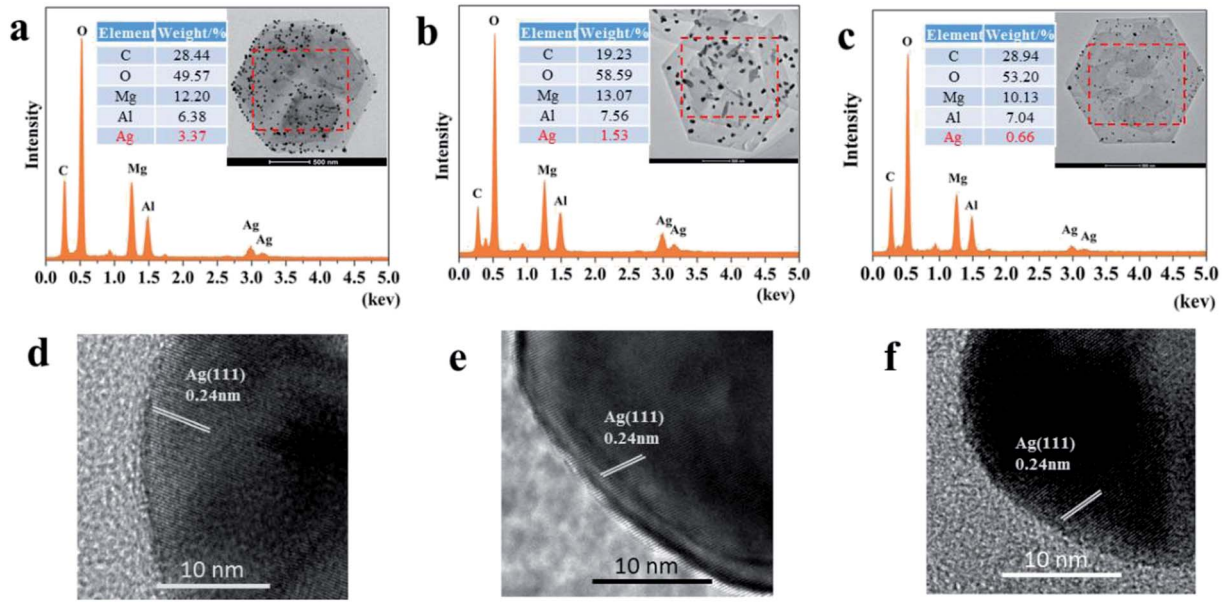

Fig. 2 EDS surface scans for (a) Ag-LDHs(PVP), (b) Ag-LDHs@PDA and (c) Ag-LDHs@TA–Fe(III). HRTEM images of (d) Ag-LDHs(PVP), (e) Ag-LDHs@PDA and (f) Ag-LDHs@TA–Fe(III).

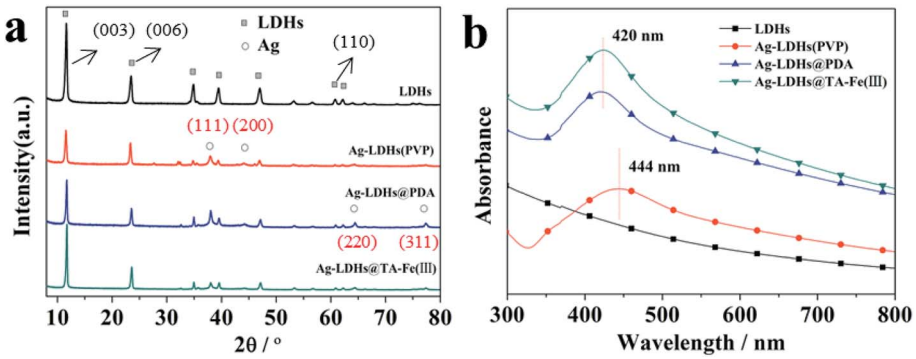

Fig. 3 (a) XRD patterns and (b) UV-vis spectra of LDHs and Ag-LDHs.

antibacterial properties. According to reports in the literature,[30,32] Ag ions released from the AgNPs contribute to the antibacterial activity. Therefore, LDHs with smaller sized AgNPs embedded in them and higher quantities of AgNP loading exhibit better antibacterial efficacy. Among the three kinds of Ag-LDHs, Ag-LDHs(PVP) exhibits the best antibacterial activity, in terms of having the lowest MIC value.

The inhibition zones of the Ag-LDHs/PCL nanocomposites against *E. coli* are shown in Fig. 6. Against *E. coli*, the inhibition zones of Ag-LDHs are observed to be 16.3, 14.1 and 15.9 mm, respectively. With an increase in inhibition zone size, materials exhibit enhanced antibacterial activity. The Ag-LDHs(PVP)/PCL nanocomposite exhibits the best antibacterial activity. Obviously, the antibacterial activity of the Ag-LDHs/PCL nanocomposite is consistent with that of Ag-LDHs.

3.3. Thermal properties of Ag-LDHs/PCL nanocomposites

DSC cooling and secondary heating curves from Ag-LDHs/PCL nanocomposites are shown in Fig. 7, and the related results from thermal analysis are listed in Table 1. As seen from Fig. 7(a) and Table 1, pure PCL exhibits a crystallization exothermic peak (T_c) at 23.8 °C, which is ascribed to the α-polymorph.[33] With the addition of Ag-LDHs, the T_c and χ values of the Ag-LDHs/PCL nanocomposites occur at higher values. Therefore, increases in T_c and χ are due to the fact that all Ag-LDHs can act as heterogeneous nucleating agents to promote the crystallization process.[34] In Fig. 7(b), the melting temperature (T_m) of pure PCL is 57.3 °C while T_m values of the Ag-LDHs/PCL nanocomposites show no obvious changes (56.5–57.1 °C). This shows that Ag-LDHs samples do not obviously affect T_m.

In order to study the relationship between LDH content and the crystallinities of the nanocomposites, Ag-LDHs@TA–Fe(III) is taken as an example to study the crystalline characteristics of Ag-LDHs/PCL nanocomposites (as shown in Fig. 8(a)). To a certain extent, the XRD patterns of Ag-LDHs@TA–Fe(III)/PCL nanocomposites further verify the results from DSC analysis. The diffraction intensities from LDHs and PCL in the nanocomposites increase simultaneously with the increase in Ag-

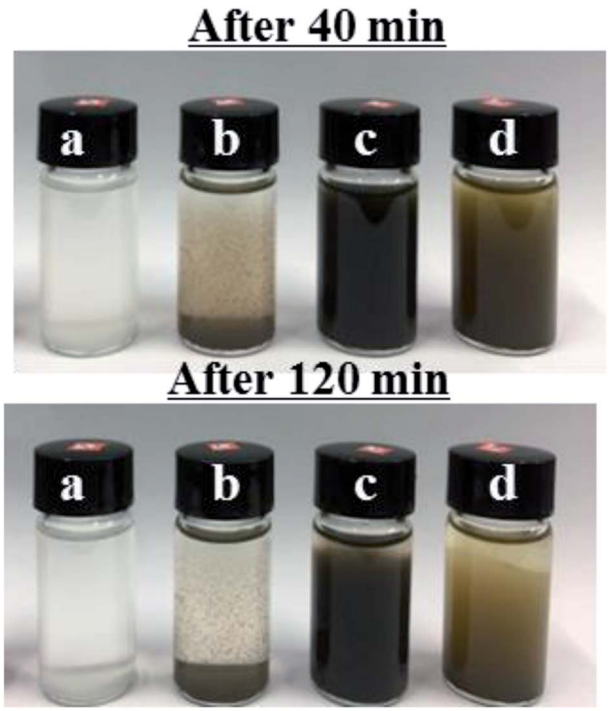

Fig. 4 Photographs of (a) LDHs, (b) Ag-LDHs(PVP), (c) Ag-LDHs@PDA and (d) Ag-LDHs@TA–Fe(III) dispersions after standing for 120 min.

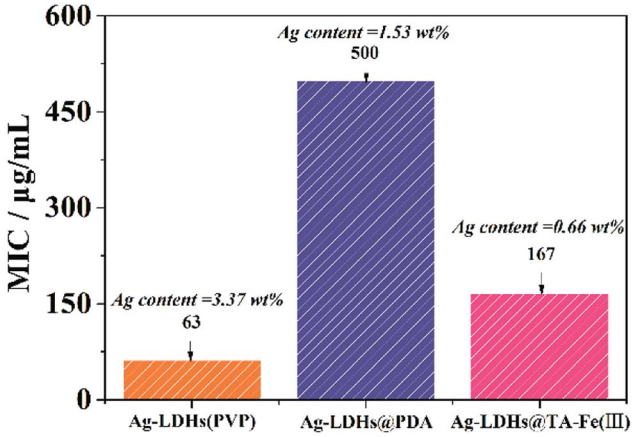

Fig. 5 The MIC values of Ag-LDHs.

LDHs@TA–Fe(III) amount. This reveals that Ag-LDHs@TA–Fe(III) facilitates the crystallization of PCL molecular chains as a result of an increase in crystallinity. It should be pointed out that the Ag-LDHs(PVP)/PCL and Ag-LDHs@PDA/PCL nanocomposites show the same trend. Therefore, Ag-LDHs can promote the crystallization process in the PCL matrix.

Fig. 8(b) shows the TGA curves from Ag-LDHs/PCL nanocomposites. According to previous studies,[33,35] the thermal degradation of LDHs/PCL nanocomposites occurs at a lower temperature in comparison with pure PCL, and the thermal degradation temperature of LDHs/PCL nanocomposites decreases gradually as the LDH loading increases. It is revealed that the thermal degradation of the Ag-LDHs(PVP)/PCL and Ag-LDHs@TA–Fe(III)/PCL nanocomposites shows the same trend. Interestingly, however, this is not the case for the Ag-LDHs@PDA/PCL nanocomposite. The Ag-LDHs@PDA/PCL nanocomposite exhibits better thermostability than pure PCL and the other Ag-LDHs/PCL nanocomposites. Owing to the high relative thermal stability of PDA, the core–shell structured Ag-LDHs@PDA contributes to a delay of the initial thermal degradation of PCL.[6] Therefore, Ag-LDHs@PDA improves the thermostability of the Ag-LDHs@PDA/PCL nanocomposite in comparison to the other Ag-LDHs/PCL nanocomposites.

3.4. Mechanical properties of Ag-LDHs/PCL nanocomposites

The mechanical properties of materials are an important factor that can decide the usability, durability and reliability of manufactured goods. Fig. 9 shows the mechanical properties of the Ag-LDHs/PCL nanocomposites. In Fig. 9(a), the tensile strength of all the Ag-LDHs/PCL nanocomposites shows a similar trend; that is, the tensile strength decreases with an increase in Ag-LDHs content. When the addition of Ag-LDHs is only 0.5 wt%, compared with pure PCL (34.4 MPa), the tensile strengths of Ag-LDHs@PDA/PCL and Ag-LDHs@TA–Fe(III)/PCL nanocomposites decrease by 4% and 11%, respectively, while the tensile strength of the Ag-LDHs(PVP)/PCL nanocomposite decreases by up to 26%. There are some differences in the elongation at break curves for all the Ag-LDHs/PCL nanocomposites (Fig. 9(b)). With an increase in Ag-LDHs content, the elongation at break for all the Ag-LDHs/PCL nanocomposites first increases and then decreases quickly. When the addition of Ag-LDHs is 0.5 wt%, the elongation at break for all the Ag-LDHs/PCL nanocomposites reaches a maximum value. However, compared with pure PCL (612%), the elongation at break values for the Ag-LDHs@PDA/PCL and Ag-LDHs@TA–Fe(III)/PCL nanocomposites increase by 50% and 39%, respectively, and the elongation at break of the Ag-LDHs(PVP)/PCL nanocomposite increases by only 25%. Therefore, compared with unmodified LDHs, the surface modification of LDHs has a remarkably positive effect on the mechanical properties of the PCL matrix.

To further understand the relationship between the material structure and mechanical properties, SEM images of the fractured surfaces of Ag-LDHs/PCL nanocomposites are shown in Fig. 10. In addition to a large number of bulges and hollows that can be observed in the fracture region (Fig. 10(a–c)), there are also numerous curled broken fibrils formed by plastic tension deformation, which can explain how the Ag-LDHs@PDA/PCL and Ag-LDHs@TA–Fe(III)/PCL nanocomposites exhibit larger elongation at break values. In Fig. 10(d–f), there is a clear gap between Ag-LDHs(PVP) and the PCL matrix, which indicates that the interfacial compatibility is relatively poor, however, Ag-LDHs@PDA and Ag-LDHs@TA–Fe(III) are both tightly combined with the PCL matrix, and there is no visible interface gap. This indicates that the interfacial compatibility is improved markedly, which can explain how the Ag-LDHs@PDA/PCL and Ag-LDHs@TA–Fe(III)/PCL nanocomposites exhibit better mechanical properties than the Ag-LDHs(PVP)/PCL nanocomposite.[6,16] Moreover, elements of suspected AgNPs on the surfaces of the

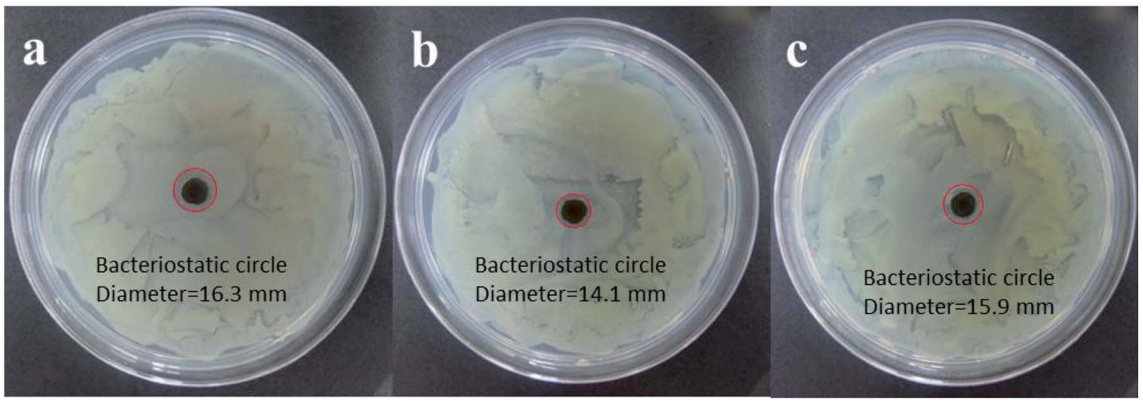

Fig. 6 The inhibition zone sizes against *E. coli* on different membranes: the (a) Ag-LDHs(PVP)/PCL nanocomposite; (b) Ag-LDHs@PDA/PCL nanocomposite; and (c) Ag-LDHs@TA–Fe(III)/PCL nanocomposite.

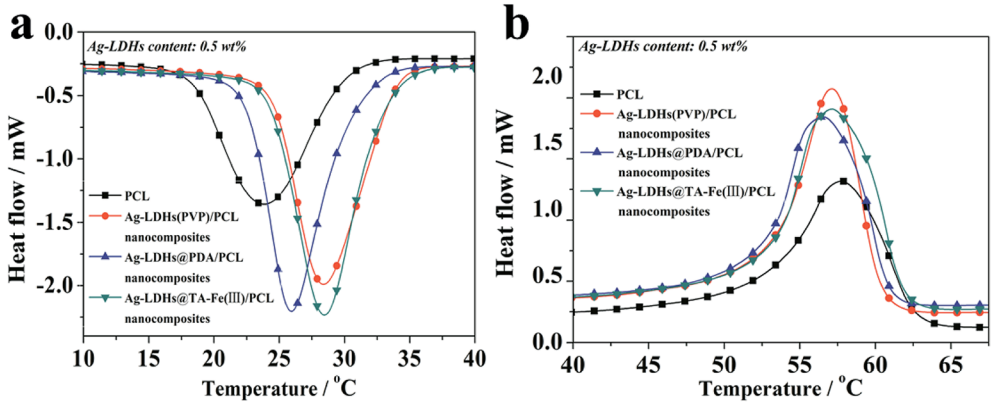

Fig. 7 DSC (a) cooling and (b) secondary heating curves of Ag-LDHs/PCL nanocomposites.

Table 1 The results for Ag-LDHs/PCL nanocomposites according to thermal analysis

Sample	ΔH_m/J g^{-1}	T_m/°C	T_c/°C	χ/%
PCL	45.18	57.3	23.8	33.2
Ag-LDHs(PVP)/PCL nanocomposite	52.70	57.1	28.4	38.9
Ag-LDHs@PDA/PCL nanocomposite	52.31	56.5	25.9	38.7
Ag-LDHs@TA–Fe(III)/PCL nanocomposite	57.94	57.1	28.5	42.8

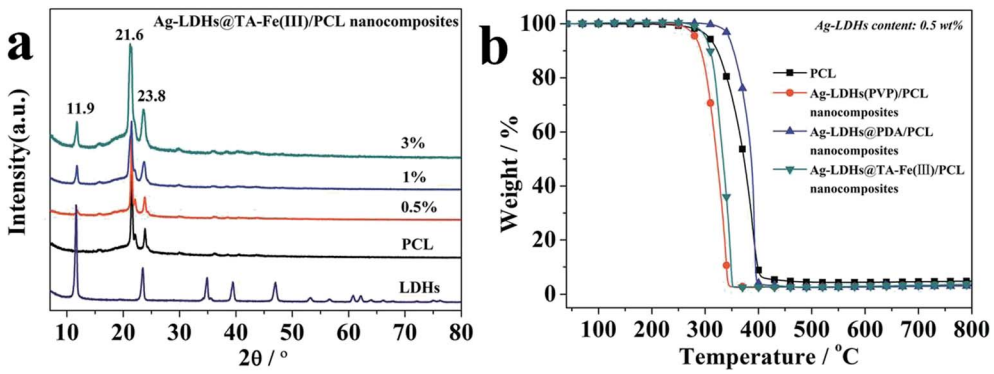

Fig. 8 (a) XRD patterns and (b) TGA curves of Ag-LDHs/PCL nanocomposites.

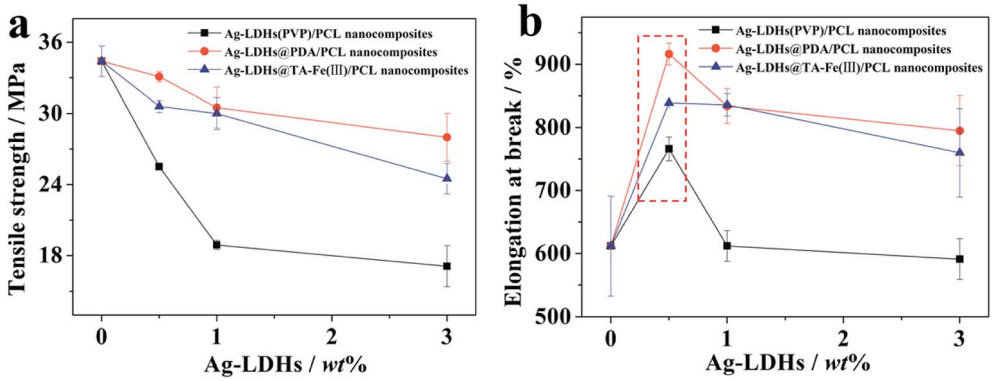

Fig. 9 The (a) tensile strength and (b) elongation at break curves for Ag-LDHs/PCL nanocomposites.

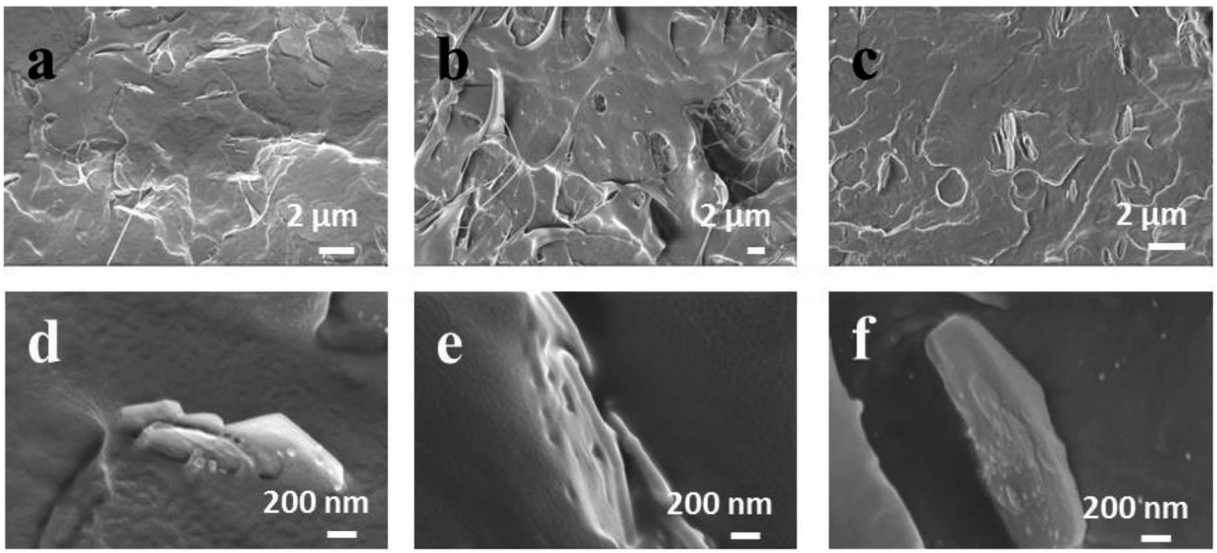

Fig. 10 SEM images of the fractured surfaces of Ag-LDHs/PCL nanocomposites at different magnifications (the Ag-LDHs content is 0.5 wt%): (a and d) Ag-LDHs(PVP)/PCL nanocomposite; (b and e) Ag-LDHs@PDA/PCL nanocomposite; and (c and f) Ag-LDHs@TA–Fe(III)/PCL nanocomposite.

LDHs are analyzed *via* EDS and the results show that Ag appears in the EDS spectra, which confirms that these spherical particles are AgNPs.

3.5. Barrier properties of Ag-LDHs/PCL nanocomposites

The oxygen permeability of the Ag-LDHs/PCL nanocomposites is shown in Fig. 11. With an increase in Ag-LDHs content, the oxygen permeabilities of all the Ag-LDHs/PCL nanocomposites decrease gradually. With the same amount of Ag-LDHs, the oxygen permeabilities of the Ag-LDHs/PCL nanocomposites show different values, which is related to the dispersion of Ag-LDHs itself in the PCL matrix and the interactions between Ag-LDHs and the PCL matrices. In particular, when the addition of Ag-LDHs reaches 3 wt%, the oxygen permeabilities of the Ag-LDHs@PDA/PCL and Ag-LDHs@TA–Fe(III)/PCL nanocomposites decrease by 27% and 26%, respectively. And their reduction values reach twice as much as that of the Ag-LDHs(PVP)/PCL nanocomposite. Combined with previous analysis, it is revealed that Ag-LDHs@PDA and Ag-LDHs@TA–

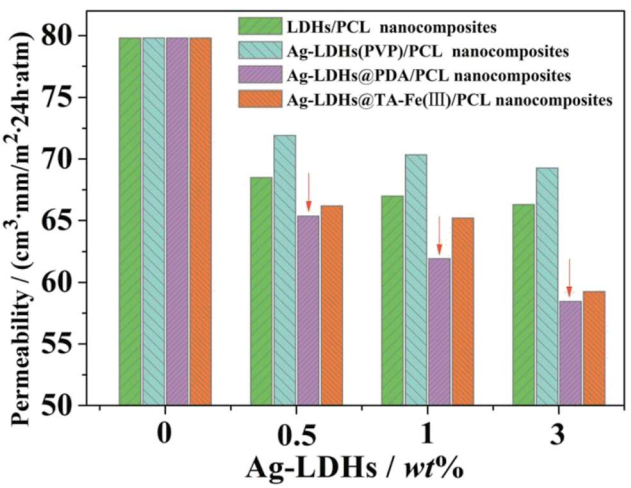

Fig. 11 The O_2 permeability of the Ag-LDHs/PCL nanocomposites.

Fe(III) are superior to Ag-LDHs(PVP) in dispersion and interface interactions. The better dispersibilities of Ag-LDHs@PDA and Ag-LDHs@TA–Fe(III) contribute to the greater aspect ratios of Ag-LDHs in the matrices, resulting in an increase in the number of tortuous paths for gas diffusion. At the same time, Ag-LDHs@PDA and Ag-LDHs@TA–Fe(III) have stronger interactions with the PCL matrix, which is favorable for the presence of less interface defects in the nanocomposites as a result of a decrease in the number density of free volume holes.[36–38] Therefore, the Ag-LDHs@PDA/PCL and Ag-LDHs@TA–Fe(III)/PCL nanocomposites show better oxygen barrier properties.

4. Conclusions

In this paper, a facile, green and mussel-inspired method was presented to prepare Ag-LDHs @PDA and Ag-LDHs@TA–Fe(III) using a pre-synthesis PDA/TA–Fe(III) layer as a nanoscale guide and PDA/TA itself as a reducing reagent to form uniform AgNPs on the surface of modified LDHs. Meanwhile, another kind of Ag-LDHs(PVP) material was prepared *via* the direct reduction of silver precursor $[Ag(NH_3)_2]^+$ ions with PVP. And three kinds of Ag-LDHs/PCL nanocomposite were prepared by blending Ag-LDHs and pure PCL *via* a solution casting method to obtain homogeneous films. It is shown that the obtained AgNPs are distributed on the LDH surface uniformly. And the high loading and medium size of the AgNPs present in Ag-LDHs(PVP) result in it showing the best antibacterial properties. Increases in crystallization temperature and crystallinity with the incorporation of Ag-LDHs into the PCL matrix is due to the fact that all the Ag-LDHs materials can act as nucleating agents with resulting heterogeneous nucleation effects. Considering the high relative thermal stability of PDA, the core–shell structured Ag-LDHs@PDA contributes to a delay in the initial thermal degradation of PCL. Compared with Ag-LDHs(PVP), the better dispersibilities of Ag-LDHs@PDA and Ag-LDHs@TA–Fe(III) contribute to the greater aspect ratios of Ag-LDHs in the matrices, resulting in an increase in the number of tortuous paths for gas diffusion. At the same time, Ag-LDHs@PDA and Ag-LDHs@TA–Fe(III) have stronger interactions with the PCL matrix, which is favorable for creating less interface defects in the matrix, resulting in increases in mechanical and gas barrier properties. Therefore, Ag-LDHs@PDA/PCL and Ag-LDHs@TA–Fe(III)/PCL nanocomposites show preferable mechanical and gas barrier properties. Thanks to the superiority of their physical properties, mussel-inspired antibacterial Ag-LDHs/PCL nanocomposites are promising materials that could be widely applied in the packaging and biomedical industries.

Conflicts of interest

The authors declare no competing financial interests.

Acknowledgements

This study was supported by the National Natural Science Foundation of China (No. 11872179 and 21704085), Science and Technology Planning Project of Fujian Province (No. 2018H6024), Young and Middle-aged Teachers Education Scientific Research Project of Fujian Province (No. JT180420 and JAT160354), Open fund of Fujian Provincial Key Laboratory of Functional Materials and Applications (Xiamen University of Technology) (No. fma2018004 and fma2017110), and Fujian Province Natural Science Fund (No. 2016J01322), Fujian Province Education Department Fund (No. JAT160351).

References

1 S. Zhao and J. Li, Silver-Cobalt Oxides Derived from Silver Nanoparticles Deposited on Layered Double Hydroxides for Methane Combustion, *ChemCatChem*, 2015, **7**(13), 1966–1974.
2 J. Leng, N. Kang, D. Wang, *et al.*, Structure-Property Relationships of Nanocomposites Based on Polylactide and Layered Double Hydroxides – Comparison of MgAl and NiAl LDH as Nanofiller, *Macromol. Chem. Phys.*, 2017, **218**(20), 1700232.
3 N. G. B. Allou, P. Saikia, A. Borah, *et al.*, Hybrid nanocomposites of layered double hydroxides: an update of their biological applications and future prospects, *Colloid Polym. Sci.*, 2017, **295**(5), 725–747.
4 C. Wang, H. Han, W. Jiang, *et al.*, Immobilization of Thermostable Lipase QLM on Core-Shell Structured Polydopamine-Coated Fe_3O_4 Nanoparticles, *Catalysts*, 2017, **7**(2), 49–60.
5 H. J. Nam, E. B. Park and D. Jung, Bioinspired polydopamine-layered double hydroxide nanocomposites: controlled synthesis and multifunctional performance, *RSC Adv.*, 2016, **6**(30), 24952–24958.
6 L. Mao, Y. Liu, H. Wu, *et al.*, Poly(ε-caprolactone) filled with polydopamine-coated high aspect ratio layered double hydroxide: simultaneous enhancement of mechanical and barrier properties, *Appl. Clay Sci.*, 2017, **150**, 202–209.
7 L. P. Si, L. Yang, S. Huang, *et al.*, Shape memory polyurethane with polydopamine-coated nanosheets: simultaneous enhancement of recovery stress and strain recovery ratio and the underlying mechanisms, *Eur. Polym. J.*, 2014, **57**(8), 11–21.
8 H. J. Nam, E. B. Park and D. Jung, Bioinspired polydopamine-layered double hydroxide nanocomposites: controlled synthesis and multifunctional performance, *RSC Adv.*, 2016, **6**(30), 24952–24958.
9 J. Xie, K. Zhang, J. Wu, *et al.*, Bio-nanocomposite films reinforced with organo-modified layered double hydroxides: preparation, morphology and properties, *Appl. Clay Sci.*, 2016, **126**, 72–80.
10 T. Xu, J. Zhang, H. Chi, *et al.*, Multifunctional properties of organic-inorganic hybrid nanocomposites based on chitosan derivatives and layered double hydroxides for ocular drug delivery, *Acta Biomater.*, 2016, **36**, 152–163.
11 Q. Song, W. Zhao, H. Yin, *et al.*, Facile synthesis of FeIII–tannic acid film-functionalized magnetic silica microspheres for the enrichment of low-abundance peptides and proteins for MALDI-TOF MS analysis, *RSC Adv.*, 2015, **5**(78), 63896–63902.

12 H. Ejima, J. J. Richardson, K. Liang, *et al.*, One-step assembly of coordination complexes for versatile film and particle engineering, *Science*, 2013, **341**(6142), 154–157.

13 M. Božič, S. Gorgieva and V. Kokol, Homogeneous and heterogeneous methods for laccase-mediated functionalization of chitosan by tannic acid and quercetin, *Carbohydr. Polym.*, 2012, **89**(3), 854–864.

14 G. Kang, M. Liu, B. Lin, *et al.*, A novel method of surface modification on thin-film composite reverse osmosis membrane by grafting poly(ethylene glycol), *Polymer*, 2007, **48**(5), 1165–1170.

15 H. J. Kim, Y. Choi, M. Lim, *et al.*, Reverse osmosis nanocomposite membranes containing graphene oxides coated by tannic acid with chlorine-tolerant and antimicrobial properties, *J. Membr. Sci.*, 2016, **514**, 25–34.

16 L. Mao, H. Wu, Y. Liu, *et al.*, Enhanced mechanical and gas barrier properties of poly(ε-caprolactone) nanocomposites filled with tannic acid-Fe(III) functionalized high aspect ratio layered double hydroxides, *Mater. Chem. Phys.*, 2018, **211**, 501–509.

17 A. Roy, B. S. Butola and M. Joshi, Synthesis, characterization and antibacterial properties of novel nano-silver loaded acid activated montmorillonite, *Appl. Clay Sci.*, 2017, **146**, 278–285.

18 F. B. Karel, A. S. Koparal and E. Kaynak, Development of Silver Ion Doped Antibacterial Clays and Investigation of Their Antibacterial Activity, *Adv. Mater. Sci. Eng.*, 2015, **2015**, 1–6.

19 H. Wu, J. Huang and Y. Liu, Polysulfone ultrafiltration membrane incorporated with Ag-SiO_2 nanohybrid for effective fouling control, *J. Water Health*, 2017, **15**(3), 341–352.

20 M. Lavorgna, I. Attianese, G. G. Buonocore, *et al.*, MMT-supported Ag nanoparticles for chitosan nanocomposites: structural properties and antibacterial activity, *Carbohydr. Polym.*, 2014, **102**(3), 385–392.

21 G. Cao, Y. Sun, J. Chen, *et al.*, Sutures modified by silver-loaded montmorillonite with antibacterial properties, *Appl. Clay Sci.*, 2014, **93–94**, 102–106.

22 A. L. Incoronato, G. G. Buonocore, A. Conte, *et al.*, Active systems based on silver-montmorillonite nanoparticles embedded into bio-based polymer matrices for packaging applications, *Journal of Food Protection*, 2010, **73**(12), 2256–2262.

23 Y. Cong, T. Xia, M. Zou, *et al.*, Mussel-inspired polydopamine coating as a versatile platform for synthesizing polystyrene/Ag nanocomposite particles with enhanced antibacterial activities, *J. Mater. Chem. B*, 2014, **2**(22), 3450–3461.

24 Z. Zhang, J. Zhang, B. Zhang, *et al.*, Mussel-inspired functionalization of graphene for synthesizing Ag-polydopamine-graphene nanosheets as antibacterial materials, *Nanoscale*, 2013, **5**(1), 118–123.

25 R. Patwa, A. Kumar and V. Katiyar, Effect of silk nano-disc dispersion on mechanical, thermal, and barrier properties of poly(lactic acid) based bionanocomposites, *J. Appl. Polym. Sci.*, 2018, **135**(38), 46671.

26 A. Boujemaoui, C. Cobo Sanchez, J. Engström, *et al.*, Polycaprolactone Nanocomposites Reinforced with Cellulose Nanocrystals Surface-Modified *via* Covalent Grafting or Physisorption: A Comparative Study, *ACS Appl. Mater. Interfaces*, 2017, **9**(40), 35305–35318.

27 L. Mao, Y. Liu, Y. Bai, *et al.*, Poly(ε-caprolactone) nanocomposites with layered double hydroxides modified by *in situ* grafting polymerization: structure characterization and barrier properties, *J. Appl. Polym. Sci.*, 2017, **134**(38), 45320–45326.

28 L. N. Ludueña, V. A. Alvarez and A. Vazquez, Processing and microstructure of PCL/clay nanocomposites, *Mater. Sci. Eng., A*, 2007, **460–461**, 121–129.

29 Y. Liu, L. Mao and S. Fan, Preparation and study of intumescent flame retardant poly(butylene succinate) using MgAlZnFe-CO_3 layered double hydroxide as a synergistic agent, *J. Appl. Polym. Sci.*, 2014, **131**(17), 8964–8973.

30 X. Wang, Z. Liang, F. Zhang, *et al.*, Enhanced catalytic performances of Ag nanoparticles supported on layered double hydroxide for styrene epoxidation, *J. Mater. Sci.*, 2013, **48**(17), 5899–5903.

31 G. Xu, X. Qiao, X. Qiu, *et al.*, Preparation and characterization of nano-silver loaded montmorillonite with strong antibacterial activity and slow release property, *J. Mater. Sci. Technol.*, 2011, **27**(8), 685–690.

32 S. C. Motshekga, S. S. Ray, M. S. Onyango, *et al.*, Microwave-assisted synthesis, characterization and antibacterial activity of Ag/ZnO nanoparticles supported bentonite clay, *J. Hazard. Mater.*, 2013, **262**(8), 439–446.

33 R. Pucciariello, L. Tammaro, V. Villani, *et al.*, New nanohybrids of poly(ε-caprolactone) and a modified Mg/Al hydrotalcite: mechanical and thermal properties, *J. Polym. Sci., Part B: Polym. Phys.*, 2007, **45**(8), 945–954.

34 H. Peng, Y. Han, T. Liu, *et al.*, Morphology and thermal degradation behavior of highly exfoliated CoAl-layered double hydroxide/polycaprolactone nanocomposites prepared by simple solution intercalation, *Thermochim. Acta*, 2010, **502**(1–2), 1–7.

35 U. Costantino, V. Bugatti, G. Gorrasi, *et al.*, New Polymeric Composites Based on Poly(ε-caprolactone) and Layered Double Hydroxides Containing Antimicrobial Species, *ACS Appl. Mater. Interfaces*, 2009, **1**(3), 668–677.

36 R. K. Layek, A. K. Das, M. J. Park, *et al.*, Enhancement of physical, mechanical, and gas barrier properties in noncovalently functionalized graphene oxide/poly(vinylidene fluoride) composites, *Carbon*, 2015, **81**(1), 329–338.

37 D. Aldana, E. Villa, M. De Dios Hernández, *et al.*, Barrier properties of polylactic acid in cellulose based packages using montmorillonite as filler, *Polymers*, 2014, **6**(9), 2386–2403.

38 S. Zekriardehani, S. A. Jabarin, D. R. Gidley, *et al.*, Effect of chain dynamics, crystallinity, and free volume on the barrier properties of poly(ethylene terephthalate) biaxially oriented films, *Macromolecules*, 2017, **50**(7), 2845–2855.